Structure conformational, molecular docking and computational investigation of Methyl Linoleate

C. Prabhu
Vels University

Rajesh Pv
School of Basic Sciences, Vels Institute of Science Technology & Advanced Studies…

Chemical Physics Impact 7 (2023) 100300

Contents lists available at ScienceDirect

Chemical Physics Impact

journal homepage: www.sciencedirect.com/journal/chemical-physics-impact

Full Length Article

Structure conformational, molecular docking and computational investigation of Methyl Linoleate

C. Prabhu [a], P. Rajesh [a,*], E. Dhanalakshmi [a,*], T. Gnanasambandan [b], M. Priyadharshini [c]

[a] Department of Physics, School of Basic Sciences, Vels Institute of Science, Technology & Advanced Studies, Pallavaram, Chennai, 600 117, Tamilnadu,India
[b] Department of Physics, Saveetha School of Engineering, Saveetha Institute of Medical and Technical Sciences (SIMATS), Thandalam, Chennai, 602105, Tamilnadu, India
[c] Department of Mathematics, SRM Institute of Science and Technology Ramapuram, Chennai, 600089, Tamil Nadu, India

ARTICLE INFO

Keywords:
Methyl Linoleate
FT-IR
UV-Vis
DFT
NBO
PES
Molecular Docking

ABSTRACT

The Methyl Linoleate, also called polyunsaturated fatty acid, is a natural drug synthesis from 100% medicinal plant of L.AegleMarmelos. The title molecules structure conformed through GC-MS results. The geometry structure parameters on the title molecule were optimized and determinate at the same level of B3LYP/6-311++G (d,p) correlated with the XRD database. Thermodynamic properties estimated at different temperatures and the NBO used to analysis inter-intra molecular interaction, the first-order hyperpolarizability were also completed. The DFT were computed NMR, energy gap reported 5.33 eV it is related to biological activity and MEP used to predict the chemical reactive site of electrophilic and nucleophilic attack. The TD-DFT executed UV-Visible spectra found at 266 nm is good agreements with experimental value and the FT-IR spectra of each vibrational mode compared with the theoretical spectra and potential energy distribution PED% carried out. The PES studies have been estimated to investigate the configuration analysis of double bond. The molecular docking found the stability of protein-ligand complex on 4HOE receptor against candida diagnosis.

1. Introduction

Methyl linoleate is one of the essential fatty acid methyl esters produced during transesterification of triglyceride oil and primary alcohol to produce biodiesel fuel. Chemicals like fatty alcohol and chlorinated methyl ester can be produced using methyl esters. Methyl esters are often used in lubricants, coatings, food and agriculture, metalworking fluids, and biofuels. Methyl esters are produced by the transesterification of vegetable oils. By dissociating aggregates and unfolding proteins, the fatty acid methyl ester methyl linoleate is used in numerous studies as a non-ionic surfactant to assist solubilizes a range of chemical species. In order to increase the solubility of substances, methyl linoleate is employed as a nonionic surfactant which dissociates aggregates and unfolds proteins. It is an emulsifier and stabiliser made of fatty acid ester. Several authors explored methyl linoleate and its derived compounds. The Rutaceae family includes the plant aegle marmelos, which has enormous therapeutic potential and the fruits of A. marmelos are used to treat diabetes, diarrhoea, dysentery, and mental illnesses in addition to high fever [1]. The organic compound methyl linoleate was synthesised from the natural plant of L. aeglemarmelos, which contains many bio compounds such as imperatorin, aegeline, coumarin and xanthotoxol those compounds used to predict against anticancer, anti-fertility, antimicrobial and antifungal activity [2]. Multiple extracts discovered from the dried leaves of A. marmelos contained phytochemicals and antioxidants [3]. The neuroprotective effects of A. marmelos leaf ethanolic extract (AME) on male rats' STZ-induced memory impairment [4]. Silver nanoparticle synthesis from L.AegleMarmelos as reducing agent [5]. Metal nitrate solution and Aegle marmelos extracts are used as precursors in the manufacture of zinc ferrite nanoparticles. To determine their properties, the created spinel nanoparticles were evaluated by UV-vis, FTIR, XRD, VSM, and FE-SEM techniques. Evaluation of the antimicrobial efficacy of zinc ferrite nanoparticles against gram-positive, gram-negative microorganisms and carfilzomib drug delivery [6]. The anti-inflammatory properties used against both acute and long-term inflammation in rats [7]. The toxicological, antioxidant, and pharmacological potentials estimated by A. marmelos [8]. The biosynthesis of silver nanoparticles from aqueous leaf extract investigated anticancer, larvicidal activity [9]. The methanol extracts of A. marmelos leaves estimate biochemical changes in antidiabetic treatment [10]. The GC-MS, NMR and HPLC analysis by ethanolic extract of

* Corresponding Authors: (P. Rajesh) & (E. Dhanalakshmi) Tel: +91 8189823556
E-mail addresses: rajesh.ncc5coy@gmail.com (P. Rajesh), jdkrishii2015@gmail.com (E. Dhanalakshmi).

https://doi.org/10.1016/j.chphi.2023.100300
Received 10 July 2023; Received in revised form 18 August 2023; Accepted 3 September 2023
Available online 9 September 2023

Aeglemarmelos leaves for antioxidant activity [11].

To the best of our knowledge, the literature survey reports the theoretical analysis (DFT) on MLL compound has not yet been done. In the current investigation, the synthesis of MLL molecules identified from the GC-MS results. The MLL molecules were studied using the B3LYP/6-311++G (d,p) technique that correlated with the spectroscopic techniques of UV-Visible and FT-IR spectrum. The relations between S, C and H were used for estimating the thermodynamic characteristics of MLL for different temperature levels. The optimized parameters values correlated with the XRD database. The inter-intra molecular interaction and charge delocalization of the title compound were analysed by the NBO technique. The energy gap (eV), chemical potential (μ), chemical softness (σ) used to predict stability and reactivity sites on MLL have been computed B3LYP/6-311++G (d,p) level. The MEP was used to predict chemical reactive sites of electrophilic and nucleophilic attack. The UV-Visible spectra absorption interpreted by TD-DFT good agreements with experimental value. The FT-IR spectra of each vibrational mode compared with the theoretical spectra and potential energy distribution PED% carried out Veda 04 software. Potential Energy Scan (PES) examination was used to investigate the conformation analysis. The molecular docking studied on the 4HOE protein against candida diagnosis.

2. Experimental techniques

The bioactive components green synthesis from methanol extract of L.AegleMarmelos, the 100% medicinal plant of L.AegleMarmelos was collected from Vels University (VISTAS), Pallavaram, Tamil Nadu, India. The bulk of 2 kg was dried at room temperature and an electric grinder was used to grind 1 kg, after using methanol to dip 2:1 ratio for absorbed compound at 48 h, utilized the soxhlet process to isolate crude and methanol. The GC-MS (QP2010 Plus – Shimadzu) at SRM University, Kattankulathur, Chengalpattu district, Tamil nadu have been analysis crude of L.AegleMarmelos, that result reported and identify many bio-components. According to the antifungal activity, we chose only one bio-compound methyl linoleate from the GC-MS result. The MLL compound purchased from Sigma-Aldrich Company with 99% purity was given to spectroscopic technique (FT-IR, UV-Vis) for functional group identification. Using the KBr pellet technique, the FT-IR spectra of MLL compound were obtained on a Perkin Elmer FT-IR spectrophotometer in the range of 4000-400 cm^{-1}. The UV-3600 plus Shimadzu instrument was used to measure the absorption of UV-Vis spectrum, which ranges from 300 to 200 nm. All spectral measurements were made at SRM University in Kattankulathur, Chengalpattu district, Tamil Nadu, India.

3. Computational Details

All theoretical calculations were done by Gaussian 09 W software [12]. The geometry parameters of bond angle and bond length interpreted hybrid functional Becke-Lee, Parr, and Yang DFT/B3LYP technique with 6-311++G (d,p) level [13,14]. The vibrational wave number of FT-IR spectra corresponding to PED% carried out by Veda 04 software, MEP plot and HOMO, LUMO are visualized by Gauss view 5.0 programmes [15,16]. Thermodynamic parameters evaluated at different temperatures obtained by THERMO.PL [17]. The calculated UV-Visible absorption spectra were examined using the TD-DFT method with hybrid B3LYP/6-311++G(d,p) level [18]. The natural bond orbital investigation (hyperconjugate interaction, charge transfer between donor, acceptor and intra-inter molecular hydrogen-bonding interaction) is interpreted by second order perturbation theory [19]. The location of the reactive site was determined through the MEP surface; the mulliken population analysis and NMR, electronic properties of the energy gap, electrophilicity index, and nucleophilicity index were also calculated [20]. The PES scan performed by B3LYP/6-311++G (d,p) and results shows GaussView 5.0 [21]. The molecular docking analysis ligand-protein interaction and binding to the receptor was computed by AutoDock Tool 1.5.6 software [22].

4. Observations and Discussion

4.1. The GC-MS investigation on L.AegleMarmelos

The gas chromatography – mass spectrometry analysis methanol extract of ***L.AegleMarmelos*** that total running time period was 21.74 min. The GC-MS results show a total of eight bio-components related to molecular weight, retention duration, and molecular formula that are found in the NIST database [23,24]. In the current investigation the GC-MS result reported eight major constituents, which mainly includes as Methyl Linoleate (MLL), Octadecanoic Acid- 17-Oxo-Methyl Ester, 9-octadecenoic acid (z)- methyl ester, Octadec-9-enoic acid, cis-11-Eicosenoic acid, methyl ester, Dodecanoic acid and Tetracosanoic acid, methyl ester related to retention time 14.15, 16.08, 17.57, 18.93, 19.45, 20.06 and 21.74 and molecular weight 294.5, 312.5, 296.5, 282.5, 324.5, 214.3 and 382.6 g/mol are listed in Table 1. These bio-components are identified and matching data are available on PubChem databases and NIST data library. The results of GC-MS revealed many components, but particularly we chose one bio-compound (MLL) as shown in Fig. 1 based on antifungal activity for further work, which is comparative studies on quantum chemical calculation, spectroscopic studies and molecular docking on Methyl Linoleate (MLL) compound respectively.

4.2. Geometry Molecular Structure on MLL Molecules

The optimized geometry molecular structure on MLL compound in gas phase and numbering of atoms are interpreted using hybrid process B3LYP with 6-311++G (d,p) level as shown in Fig. 2. The molecule belongs to the C_1 symmetry point group, and the estimated frequency indicates that it is an A symmetry species [25,26]. The structural parameters of MLL molecules such as bond length, bond angle were determined and are given in Table 2. In the title molecules, the smallest bond length 1.09 in C_2-H_{22} represented the strongest bond in the molecules and the largest bond length 1.54 in C_{14}-C_{15} which denoted weakest bond in the MLL molecules. The carbon-oxygen (CO_2) is an electron donating group, carbon-hydrogen (CH_3) electron accepting group and the crystal structure (XRD) of the methyl linoleate compound is not available in crystallography, so the similar structure can only correlated with optimized structure on MLL molecules as shown Table 2 [27].

The minimum configuration analysis has been interpreted through the potential energy surface by using the B3LYP/6-311++G (d,p) technique, as shown in Fig. 3. [28]. In the current investigation, three dimensional optimized structures with minimum energy on the methyl linoleate compound identified the stable conformation at torsional angle (O_{19}-C_1-O_{20}-$C2_1$) [21]. The local minimum energy observed at the point of 160 scan coordinator with -0.230 total energy (Hartree), which

Table 1
Report on bioactive compounds from *L.AegleMarmelos*

Name of the Compound	Molecular Formula (MF)	Molecular weight (MW)	Retention time (RT)
Methyl Linoleate (MLL)	$C_{19}H_{34}O_2$	294.5 g/mol	14.15
Octadecanoic Acid- 17-Oxo-Methyl Ester	$C_{19}H_{36}O_3$	312.5 g/mol	16.08
9-octadecenoic acid (z)- methyl ester	$C_{19}H_{36}O_2$	296.5 g/mol	17.57
Octadec-9-enoic acid	$C_{18}H_{34}O_2$	282.5 g/mol	18.93
cis-11-Eicosenoic acid, methyl ester	$C_{21}H_{40}O_2$	324.5 g/mol	19.45
Dodecanoic acid, methyl ester	$C_{13}H_{26}O_2$	214.3 g/mol	20.06
Tetracosanoic acid, methyl ester	$C_{25}H_{50}O_2$	382.6 g/mol	21.74

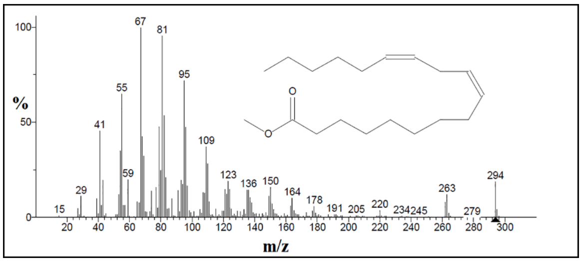

Fig. 1. GC-MS result of MLL Compound

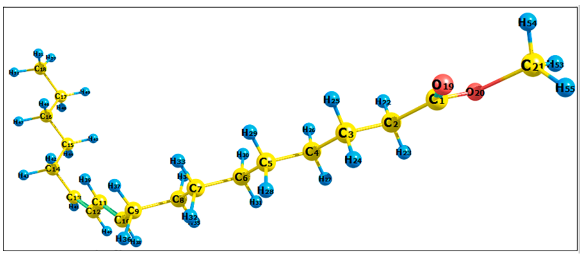

Fig. 2. Optimized Structure on MLL Compound

represents more stable conformation, and the local maximum energy conformed at 75 scan coordinator with -0.226 Hartree energy, which denotes less stable conformation on MLL molecules in the torsional angle (O_{19}-C_1-O_{20}-$C2_1$), respectively.

4.3. Vibrational spectral analysis

In addition to other fields of research, vibrational spectroscopy has contributed to important discoveries in numerous areas of chemistry and physics. The molecule of the MLL chemical has 55 atoms and 159 normal modes of vibration and belongs to the C1 point symmetry point group [29]. The fundamental modes of vibration are determined by the hybrid method B3LYP/6-311++G (d,p) level and potential energy distribution (PED%) calculated by Veda 04 software are listed in Table 3. The observed wavenumber in experimental infra-red spectrum data and theoretical calculation values on the MLL compound are given in Fig. 4, respectively.

4.3.1. C-C band vibration

Typically, the C-C stretching vibration occurs between 1600 and 1400 cm^{-1} [30]. In this investigation, the C-C oscillating frequency bands in the MLL compound appeared in the region 1663 cm^{-1} with high intensity in the spectrum of FT-IR . The theoretical FT-IR spectra have been measured at range 1658 cm^{-1} with 45% PED contributions and the average variance among between the experimental and theoretical prediction value is only 5 cm^{-1}. That appears the quantum chemical calculation has compared and well correlated with experimental FT-IR spectra, respectively.

4.3.2. C=O Oscillating Frequency

The literature survey C=O oscillating frequency observed actively in the FT-IR spectrum reported in 1600–1850 cm^{-1} [31]. In the current study, the C=O band vibration on the title compound absorption region in 1827 cm^{-1} is exhibited in the FT-IR spectrum with medium intensity. The corresponding DFT calculation interpreted B3LYP/6-311++G(d,p) set at area 1825 cm^{-1} with 62% PED contribution. Both experimental and calculated C=O vibration data have been compared and are in good agreement with each other.

4.3.3. C-C Oscillating Frequency

The C-C oscillating frequency was strongly assigned in the previous

Table 2
Optimized Structure of Parameters on MLL Molecules

Bond length (Å)	B3LYP \6-311++G (d,p)	Experimental	Bond length (Å)	B3LYP\6-311++G (d,p)	Experimental
C_1-C_2	1.51	1.50	C_{10}-C_{11}	1.34	1.35
C_1-O_{19}	1.21	1.22	C_{10}-H_{38}	1.09	0.93
C_1-O_{20}	1.35	1.38	C_{11}-C_{12}	1.45	1.43
C_2-C_3	1.52	1.50	C_{11}-H_{39}	1.08	0.93
C_2-H_{22}	1.09	0.98	C_{12}-C_{13}	1.34	1.35
C_2-H_{23}	1.09	0.99	C_{12}-H_{40}	1.09	0.97
C_3-C_4	1.53	1.52	C_{13}-C_{14}	1.50	-
C_3-H_{24}	1.09	0.97	C_{13}-H_{41}	1.09	-
C_3-H_{25}	1.09	0.97	C_{14}-C_{15}	1.54	-
C_4-C_5	1.53	1.52	C_{14}-H_{42}	1.09	0.93
C_4-H_{26}	1.09	0.97	C_{14}-H_{43}	1.10	0.93
C_4-H_{27}	1.09	0.97	C_{15}-C_{16}	1.53	1.52
C_5-C_6	1.53	1.50	C_{15}-H_{44}	1.09	0.93
C_5-H_{28}	1.09	0.96	C_{15}-H_{45}	1.09	0.93
C_5-H_{29}	1.09	0.96	C_{16}-C_{17}	1.53	-
C_6-C_7	1.53	1.51	C_{16}-H_{46}	1.09	-
C_6-H_{30}	1.09	-	C_{16}-H_{47}	1.09	-
C_6-H_{31}	1.09	-	C_{17}-C_{18}	1.53	1.51
C_7-C_8	1.53	1.51	C_{17}-H_{48}	1.09	-
C_7-H_{32}	1.09	0.97	C_{17}-H_{49}	1.09	-
C_7-H_{33}	1.09	0.97	C_{18}-H_{50}	1.09	-
C_8-C_9	1.54	1.51	C_{18}-H_{51}	1.09	-
C_8-H_{34}	1.09	0.93	C_{18}-H_{52}	1.09	-
C_8-H_{35}	1.09	0.93	O_{20}-C_{21}	1.43	1.46
C_9-C_{10}	1.50	1.51	C_{21}-H_{53}	1.09	-
C_9-H_{36}	1.10	-	C_{21}-H_{54}	1.09	-
C_9-H_{37}	1.09	-	C_{21}-H_{55}	1.92	-
C_2-C_1-O_{19}	125.85	124.2	H_{36}-C_9-H_{37}	106.34	-
C_2-C_1-O_{20}	110.85	109.5	C_9-C_{10}-C_{11}	125.30	-
O_{19}-C_1-O_{20}	123.28	125.8	C_9-C_{10}-H_{38}	116.11	-
C_1-C_2-C_3	113.18	113.8	C_{11}-C_{10}-H_{38}	118.57	119.8
C_1-C_2-H_{22}	107.67	107.9	C_{10}-C_{11}-C_{12}	123.87	-
C_1-C_2-H_{23}	107.74	107.9	C_{10}-C_{11}-H_{39}	118.30	119.8
C_3-C_2-H_{22}	111.24	-	C_{12}-C_{11}-H_{39}	117.81	-
C_3-C_2-H_{23}	111.29	-	C_{11}-C_{12}-C_{13}	127.28	-
H_{22}-C_2-H_{23}	105.30	-	C_{11}-C_{12}-H_{40}	115.14	-
C_2-C_3-C_4	112.77	-	C_{13}-C_{12}-H_{40}	117.57	-
C_2-C_3-H_{24}	109.10	109.5	C_{12}-C_{13}-C_{14}	127.84	-
C_2-C_3-H_{25}	109.09	109.5	C_{12}-C_{13}-H_{41}	117.30	-
C_4-C_3-H_{24}	109.96	109.5	C_{14}-C_{13}-H_{41}	114.84	-
C_4-C_3-H_{25}	109.95	109.5	C_{13}-C_{14}-C_{15}	112.79	-
H_{24}-C_3-H_{25}	105.70	-	C_{13}-C_{14}-H_{42}	111.09	-
C_3-C_4-C_5	113.20	-	C_{13}-C_{14}-H_{43}	108.94	-
C_3-C_4-H_{26}	109.44	109.4	C_{15}-C_{14}-H_{42}	109.28	-
C_3-C_4-H_{27}	109.48	109.4	C_{15}-C_{14}-H_{43}	108.35	-
C_5-C_4-H_{26}	109.26	109.4	H_{42}-C_{14}-H_{43}	106.10	-
C_5-C_4-H_{27}	109.27	109.4	C_{14}-C_{15}-C_{16}	113.21	-
H_{26}-C_4-H_{27}	105.90	-	C_{14}-C_{15}-H_{44}	109.22	-
C_4-C_5-C_6	113.56	-	C_{14}-C_{15}-H_{45}	108.94	-

(*continued on next page*)

Table 2 (*continued*)

Bond length (Å)	B3LYP \6-311++G (d,p)	Experimental	Bond length (Å)	B3LYP\6-311++G (d,p)	Experimental
C_4-C_5-H_{28}	109.22	109.5	C_{16}-C_{15}-H_{44}	109.43	-
C_4-C_5-H_{29}	109.22	109.5	C_{16}-C_{15}-H_{45}	109.70	-
C_4-C_5-H_{28}	109.33	109.5	H_{44}-C_{15}-H_{45}	106.05	-
C_6-C_5-H_{29}	109.27	109.5	C_{15}-C_{16}-C_{17}	113.56	-
H_{28}-C_5-H_{29}	105.92	-	C_{15}-C_{16}-H_{46}	109.29	109.5
C_5-C_6-C_7	113.48	-	C_{15}-C_{16}-H_{47}	109.35	109.5
C_5-C_6-H_{30}	109.26	-	C_{17}-C_{16}-H_{46}	109.19	109.5
C_5-C_6-H_{31}	109.31	-	C_{17}-C_{16}-H_{47}	109.22	109.5
C_7-C_6-H_{30}	109.26	-	H_{46}-C_{16}-H_{47}	105.92	-
C_7-C_6-H_{31}	109.28	-	C_{16}-C_{17}-C_{18}	113.22	-
H_{30}-C_6-H_{31}	105.94	-	C_{16}-C_{17}-H_{48}	109.21	-
C_6-C_7-C_8	113.53	-	C_{16}-C_{17}-H_{48}	109.20	-
C_6-C_7-H_{32}	109.30	-	C_{18}-C_{17}-H_{48}	109.48	-
C_6-C_7-H_{33}	109.25	-	C_{18}-C_{17}-H_{49}	109.48	-
C_8-C_7-H_{32}	109.29	109.8	H_{48}-C_{17}-H_{49}	105.97	-
C_8-C_7-H_{33}	109.24	109.8	C_{17}-C_{18}-H_{50}	111.49	-
H_{32}-C_7-H_{33}	105.93	109.8	C_{17}-C_{18}-H_{51}	111.18	-
C_7-C_8-C_9	113.17	109.8	C_{17}-C_{18}-H_{52}	111.20	-
C_7-C_8-H_{34}	109.70	-	H_{50}-C_{18}-H_{51}	107.65	-
C_7-C_8-H_{35}	109.43	-	H_{50}-C_{18}-H_{52}	107.64	-
C_9-C_8-H_{34}	108.97	107.8	H_{51}-C_{18}-H_{52}	107.46	-
C_9-C_8-H_{35}	109.22	108.8	C_1-O_{20}-C_{21}	115.26	-
H_{34}-C_8-H_{35}	106.07	-	O_{20}-C_{21}-H_{53}	105.70	-
C_8-C_9-C_{10}	113.25	-	O_{20}-C_{21}-H_{54}	110.71	109.8
C_8-C_9-H_{36}	108.30	107.8	O_{20}-C_{21}-H_{55}	110.70	109.8
C_8-C_9-H_{37}	109.55	-	H_{53}-C_{21}-H_{54}	110.51	-
C_{10}-C_9-H_{36}	109.43	-	H_{53}-C_{21}-H_{55}	110.51	-
C_{10}-C_9-H_{37}	109.70	-	H_{54}-C_{21}-H_{55}	108.67	109.8

review at area 1590-1000 cm^{-1} [32]. In the title molecules C-C oscillating frequency observed bands are exhibit at 1069, 1118 and 1198 cm^{-1} in infra-red spectrum and all three bands are expected range reported with minimum intensity. While the calculated FT-IR spectra on C-C oscillating vibrations are recorded in the region at 1060, 1118 and 1197 cm^{-1} appeared with mixed modes of potential energy distribution (PED%). The mean value different between theoretical and experimental on the C-C band appears at 3.3 cm^{-1} that show both spectra have compared and well correlated successively.

4.3.4. C-H Oscillating Frequency

In the literature survey, the C-H oscillating frequency occurred in the range of 3250–2950 cm^{-1} [33]. In the present investigation on C-H band vibrations totally seven predictions are assigned in the region at 3180, 3162, 3135, 3094, 3080, 3068 and 3057 cm^{-1} with strong intensity in the infrared spectrum. The theoretical prediction of C-H stretching frequency observed bands at 3172, 3159, 3139, 3097, 3079, 3070 and 3052 cm^{-1} with corresponding PED with high and medium percentage appear in the MLL compound. Both wave numbers show good agreement with the observed spectral and literature data respectively.

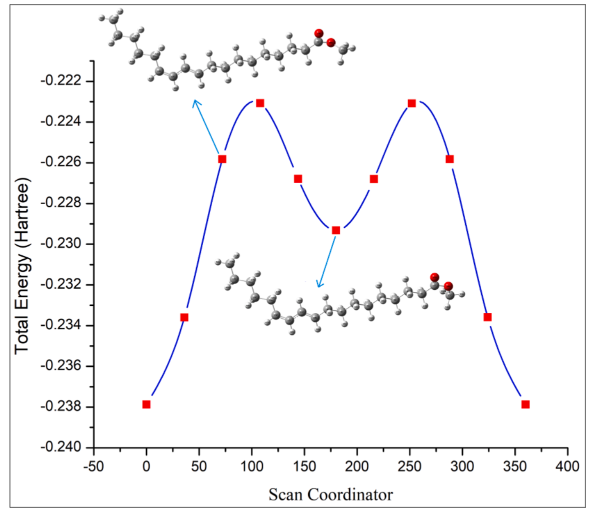

Fig. 3. Potential Energy Surface Curve of MLL

4.4. NBO analysis

Normally, the natural bond orbital is a very useful tool for investigating (hyperconjugate interaction, charge transfer between donor, acceptor and intra-inter molecular hydrogen-bonding interaction) with in molecular system have been obtained by B3LYP/6-311++G(d,p) level of quantum chemical theory [34]. The bonding (σ, π) and nonbonding (σ*, π*) interaction gaps used to identify based on the Lewis structure and the donor interaction represent Lewis-type occupied NBOs (bonding) and the acceptor interaction indicate non Lewis-type unoccupied NBOs (non-bonding) both energy interactions are used to interpret by second order perturbation theory [35]. In this study the strong hyper conjugate interaction of the **MLL** molecule was expected from the lone pairs (donor) (LP) O_{20} and (LP) C_{19} that exhibit anti-bonding pair (acceptor) π*C_1-O_{19} and σ*C_1-C_{20} with stabilization energies 49.20, 34.26 Kcal/mol both donor-acceptor interactions are occur more electron density in MLL molecular system as shown in Table 4 which is denoted by strong intermolecular charge transfer (ICT) in the MLL compound that molecules related to more biological activity. On the other hand, the minimum electron density energy transfer between bonding pairs (σ) to anti-bonding pair (σ*) intermolecular orbital interactions σC_{10}-H_{38}→ σ*C_{11}-H_{39} and σC_{11}-H_{39}→ σ*C_{10}-H_{38} with stabilization energy E(2) values 4.81 and 4.57 Kcal/mol, those donor-acceptor interactions assigned less electron density in the title compound respectively.

4.5. Muliken Population Analyses

The mulliken population analysis depends on the electron density of three dimensional on each atom in MLL molecules computed by the Gaussian 09 program in the DFT/B3LYP approach with 6-311++G (d,p) level as given in Table 5 [36,37]. The current study on MLL molecules describes the charge distribution with in the molecules, in that the whole hydrogen atoms predict as electropositive charge such as H_{22}, H_{23}, H_{52}, H_{53}, H_{54} and H_{53} with atomic charge 0.130, 0.129, 0.101, 0.118, 0.128 and 0.128 a.u and the highest electron density in hydrogen molecules has H_{23}→ 0.129 a.u as shown in Fig. 5 because (CH_2-C) which is

Table 3
Vibrational Assignment on MLL compound

B3LYP/6-311++G (d,p)	Experimental	Vibrational Assignments+(PED)
3172	3180	υCH(79)
3159	3162	υCH(70)
3153	-	υCH(99)
3139	3135	υCH(50)
3132	-	υCH(44)
3127	-	υCH(88)
3111	-	υCH(72)
3106	-	υCH(46)
3097	3094	υCH(46)
3088	-	υCH(77)
3079	3080	υCH(48)
3072	-	υCH(32)
3070	3068	υCH(93)
3066	-	υCH(27)
3056	-	υCH(55)
3055	-	υCH(49)
3052	3057	υCH(81)
3042	-	υCH(82)
3038	-	υCH(91)
3037	-	υCH(67)
3033	-	υCH(35)
3028	-	υCH(77)
3026	-	υCH(58)
3022	-	υCH(47)
3020	-	υCH(78)
3012	-	υCH(88)
3011	-	υCH(167)
3008	-	υCH(64)
3007	-	υCH(81)
3001	-	υCH(95)
1825	1827	υOC(62)
1731	1728	υCC(62) +δHCC(10)
1658	1663	υCC(45)
1528	1530	δHCH(44)
1527	-	δHCH(41)
1519	-	δHCH(41)
1518	-	δHCH(63)
1514	1514	δHCH(38)+τHCCC(14)
1511	1511	δHCH(70)
1509	-	δHCH(24)
1506	-	δHCH(62)
1501	-	δHCH(89)
1500	-	δHCH(176)
1497	1496	δHCH(80)
1495	-	δHCH(81)
1491	1490	δHCH(78)
1483	1480	δHCH(74)
1475	1472	δHCH(85)
1454	-	δHCC(65)
1428	1432	δHCH(91)
1422	-	τHCCC(22)
1418	-	τHCCC(28)
1414	-	τHCCC(22)
1410	-	τHCCC(23)
1391	-	τHCCC(11)
1389	1381	τHCCC(12)
1363	-	τHCCC(15)
1350	1348	δHCC(16)
1343	-	δHCC(22)
1342	-	δHCC(26)
1340	-	δHCC(32)
1337	1336	δHCC(15)
1335	-	δHCC(34)
1331	-	δHCC(26)
1329	-	δHCC(17)
1324	-	δHCC(13)
1315	-	δHCC(15)
1299	-	δHCC(22)
1287	-	δHCC(13)
1277	-	δHCC(11)
1261	-	τHCCC(23)
1215	1213	υOC(10)+ δHCH(13)+τHCOC(23)
1200	-	δOCO(11)
1197	1198	υCC(14)
1179	1179	δHCH(13) +τHCOC(39)
1137	-	τHCCO(14)
1118	1118	υCC(14)
1097	1096	δHCC(14)
1077	-	υCC(30)
1070	-	υCC(41)
1068	1069	υCC(51)
1066	-	υCC(26)
1053	-	υCC(13)
1045	-	υCC(42)
1042	-	υCC(39)
1030	-	τHCCC(59)
1024	-	υOC(19)
1016	-	υOC(11)
1011	-	υCC(16)
1000	998	υCC(15)
987	-	υCC(16)
984	-	τHCCC(13)+ τCCCC(10)
965	962	υCC(23)
901	-	υOC(52)

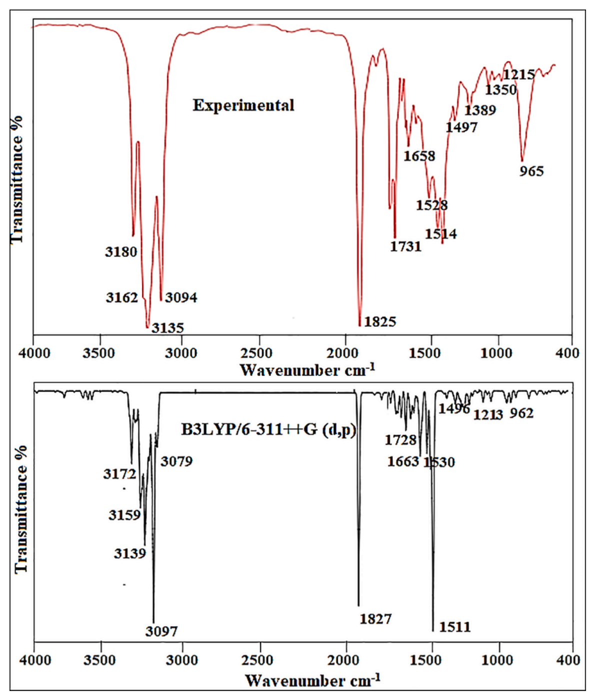

Fig. 4. FT-IR Simulated Spectrum of MLL

Table 4
Donor and Acceptor interaction NBOs analysis on MLL molecules

Donor NBO (i)	Acceptor NBO (j)	E(2) Kcal / mol	E(j) - E(i) a.u.	F(i,j) a.u.
$\sigma C_2 - H_{22}$	$\pi^* C_1 - O_{19}$	4.86	0.51	0.047
$\sigma C_2 - H_{23}$	$\pi^* C_1 - O_{19}$	4.76	0.51	0.046
$\pi C_{10} - C_{11}$	$\pi^* C_{12} - C_{13}$	15.66	0.32	0.063
$\sigma C_{10} - H_{38}$	$\sigma^* C_{11} - H_{39}$	4.81	0.98	0.061
$\sigma C_{11} - H_{39}$	$\sigma^* C_{10} - H_{38}$	4.57	0.98	0.060
$\pi C_{12} - C_{13}$	$\pi^* C_{10} - C_{11}$	14.03	0.31	0.059
$\sigma C_{12} - H_{40}$	$\sigma^* C_{13} - C_{14}$	6.31	0.94	0.069
$\sigma C_{13} - H_{41}$	$\sigma^* C_{11} - C_{12}$	6.35	1.02	0.072
(LP)O_{19}	$\sigma^* C_1 - C_2$	19.06	0.65	0.101
(LP)O_{19}	$\sigma^* C_1 - O_{20}$	34.26	0.63	0.132
(LP)O_{20}	$\pi^* C_1 - O_{19}$	49.20	0.33	0.114

Table 5
Mulliken atomic Charge on MLL molecules

Atoms	Charges (eV)	Atoms	Charges (eV)
C_1	0.607	H_{29}	0.091
C_2	-0.268	H_{30}	0.088
C_3	-0.166	H_{31}	0.088
C_4	-0.179	H_{32}	0.089
C_5	-0.175	H_{33}	0.089
C_6	-0.175	H_{34}	0.097
C_7	-0.173	H_{35}	0.090
C_8	-0.172	H_{36}	0.101
C_9	-0.216	H_{37}	0.093
C_{10}	-0.075	H_{38}	0.074
C_{11}	-0.058	H_{39}	0.069
C_{12}	-0.075	H_{40}	0.072
C_{13}	-0.088	H_{41}	0.077
C_{14}	-0.210	H_{42}	0.094
C_{15}	-0.172	H_{43}	0.101
C_{16}	-0.165	H_{44}	0.089
C_{17}	-0.174	H_{45}	0.098
C_{18}	-0.317	H_{46}	0.087
O_{19}	-0.479	H_{47}	0.087
O_{20}	-0.467	H_{48}	0.091
C_{21}	-0.082	H_{49}	0.092
H_{22}	0.130	H_{50}	0.099
H_{23}	0.129	H_{51}	0.101
H_{24}	0.108	H_{52}	0.101
H_{25}	0.109	H_{53}	0.118
H_{26}	0.088	H_{54}	0.128
H_{27}	0.087	H_{55}	0.128
H_{28}	0.090		

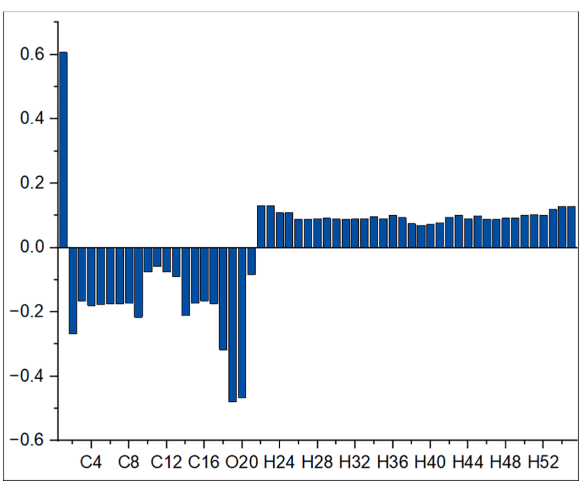

Fig. 5. Illustrate Atomic Charges of $C_{19}H_{34}O_2$ molecules

connected to the two oxygen atoms. Similarly, both oxygen atoms have the highest net electronegative charge O_{19} →-0.479 and O_{20} →-0.467 a.u in the title compound. Amongst all carbon atoms, the C_1 atom has more net positive charge 0.607 a.u and high net negative charge C_{18}→-0.317 a.u in MLL compound, respectively.

4.6. MEP plot analysis

The molecular electrostatic potential surface describes the size, shape, and reactivity of chemical molecules in electrophilic and nucleophilic reactions, and the MEP is related to the net electrostatic potential, which produces the total charge distribution of the molecular system with electron and proton [38,39]. In the title molecules, the carbon dioxide group has a high reactivity site (electrophilic attack) based on the red colour region localised, which is denoted by negative electrostatic potential, and the methyl group has a high reactivity site (nucleophilic attack) according to the blue colour region occupied, which represents positive electrostatic potential in the MLL compound, as shown in Fig. 6. On the MEP surface, the carbon-oxygen has donated the electrons, and the carbon- hydrogen accepts the electron, which is highly related to the good biological activity present in the title molecules, respectively.

4.7. Frontier Molecular Orbital

Electronic parameters such as HOMO, LUMO and energy gap are used to predict the strength, stability and reactivity of drug molecules interpreted by the DFT/B3LYP/6-311++G(d,p) method [40]. The HOMO represents the ability to donate the electron, which appears as red colour, the LUMO indicates the ability to accept the electron, which appears as green colour and the energy gap is used to describe the soft and hard materials [41]. In the current study, the HOMO has occupied the centre position in the MLL compound, and that functional group is C-H, which is denoted by donor-electrons. Similarly, the LUMO occupies the midposition in the title molecules, where the functional group is C-H, which is represented by acceptor-electrons like π-π* transition. The Koopmans's theorem used to get electronic properties values such as HOMO = -5.331 eV, LUMO = -0.324 eV, and the energy gap = 5.331 eV as shown in Fig. 7, indicates high stability and low relativity in the MLL molecular system. Additionally, electronegativity (χ), electrophilicity Index (ω), chemical harness (η) and softness (σ) are listed in Table 6 successively

4.8. UV-Visible spectra on MLL molecules

The UV-Visible spectra and related properties of oscillation strengths (f), excitation energy (eV), and absorption band (nm) have been interpreted by quantum chemical theory in the DFT/B3LYP/6-311++G(d,p) method as calculated in gas phase and correlated with experimental UV-Visible spectra [42]. In the current investigation, the electron transition 225.75 nm, excitation energy = 5.4921 eV, and oscillation strength f = 1.1322 are well correlated with experimental UV-Visible spectra absorption 226 nm, as shown in Fig. 8, which is $\pi\rightarrow\pi$* electronic transition from ground state to excited state in MLL compound, and other absorption 212.51 and 210.92 nm transitions do not coincide with the experimental values listed in Table 7, respectively. The absorption band of wavelength is 225.75 nm, which is related the major contribution HOMO→ LUMO (99%) obtained by GaussSum software. likewise, the wavelength of absorption bands have 212.51 nm and 210.92 nm corresponding H-1->L+1 (98%) and HOMO->L+1 (99%) on the title molecules.

4.9. Thermodynamic Properties

The typical thermodynamic parameters such as entropy (S), enthalpy

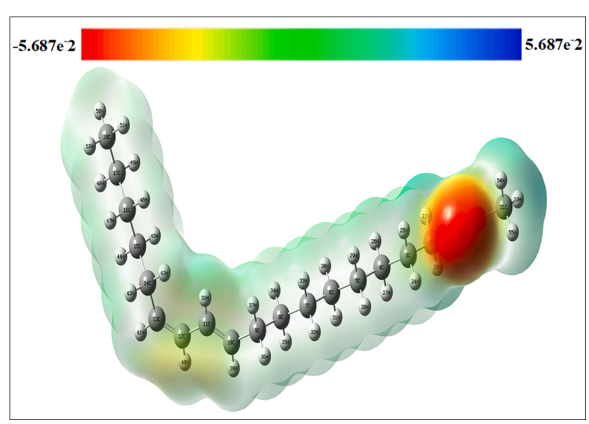

Fig. 6. MEP plot on MLL Compound

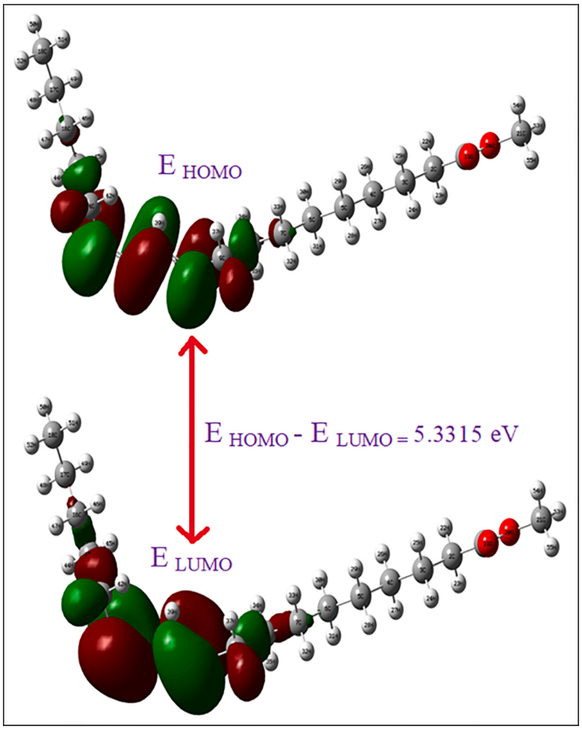

Fig. 7. HOMO, LUMO diagram on MLL molecules

Table 6
Electronic parameters calculated on MLL molecules

S.NO	Electronic parameters	B3LYP/6-311++G(d,p)
1	E_{HOMO} (eV)	-5.33 (eV)
2	E_{LUMO} (eV)	-0.32 (eV)
3	E_{HOMO}- E_{LUMO} (eV)	5.33 (eV)
4	Ionization potential (IP)	5.65 (eV)
5	Electron affinity (EA)	0.32 (eV)
6	Electronegativity (χ)	-4.38 (eV)
7	Chemical potential(μ)	4.38 (eV)
8	Chemical hardness(η)	2.66 (eV)
9	Chemical softness(σ)	0.31 (eV^{-1})
10	Electrophilicity Index(ω)	1.67 (eV)

(H), and heat capacity (C) on MLL compounds are interpreted by stand-alone Perl-Script (thermol.pl) and the Gaussian output hybrid function B3LYP/6-311++G (d,p) level as given in Table 8 [43]. The thermodynamic functions observed by entropy, enthalpy, and heat capacity have been increased. Similarly, the temperature also rose, ranging from 100K to 1000K, as shown in Fig. 9 [44], while the molecular oscillating intensity also rose with temperature on the title compound. The thermal properties have increased the temperature, which shows randomness in molecules, the energy distribution in the vibration of particles, and the chemical reactivity and good temperature of the MLL molecules.

5.0. Magnetic resonance analysis on MLL

Nuclear magnetic resonance, commonly referred to as NMR, is a technology with enormous opportunities for examining molecular structure designs, and it is frequently used in the chemical and drug sectors for clarifying the structures of medicines and other components [45,46]. In the current investigation on MLL compounds, chemical shift values of proton and carbon NMR in DMSO were calculated by using the GIAO technique through DFT/B3LYP/6-311++G (d,p) level as shown in Table 9 [47,48]. The linear structure of the MLL compound was observed in C NMR at 13.13–155.01 ppm and in proton NMR at 2.33–7.95 ppm. The theoretical C NMR chemical shift values in the carbonyl group have their highest values in the region C1 = 155.01 ppm due to the impact of carbon atoms connected with neighbouring electronegative oxygen atoms, which determines the flow of electrons. The chemical shift H NMR value was estimated at H39 = 7.95 ppm, which connected to C=C and C-C on the title molecules. The commuted chemical shift values of methyl and methylene confirm the presented MLL compound, respectively.

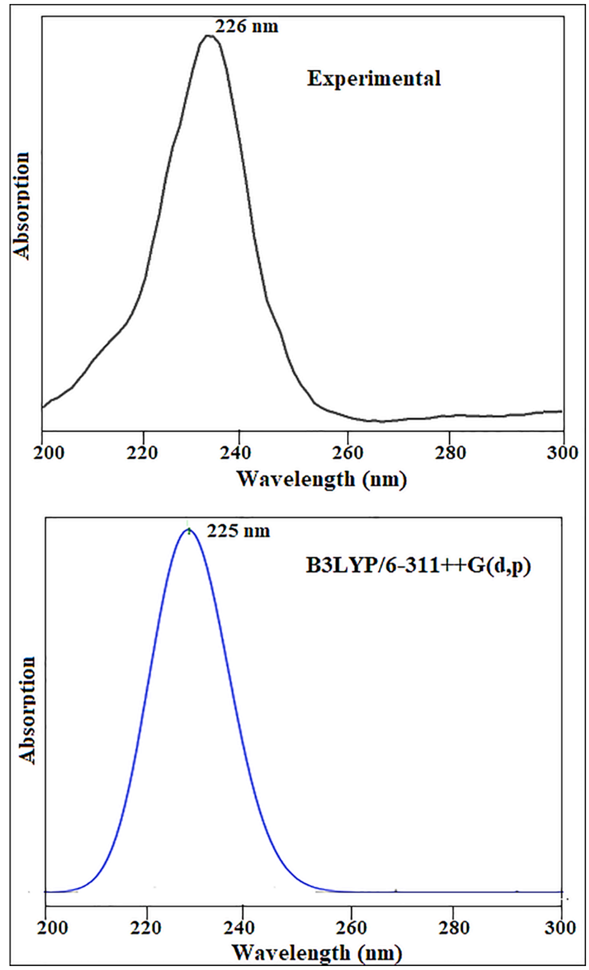

Fig. 8. UV-Vis Spectra on MLL molecules

5.1. Molecular Docking on MLL compound

Molecular docking is an efficient tool for investigating biological drug materials with ligand-protein interaction and binding to the receptor, which is a three dimensional structure computed by AutoDock Tool 1.5.6 software docking analysis [49,50]. In the present investigation, the green synthesis of the MLL ligand selected the active receptor 4HOE protein, which is classified under Candida albicans. The ligand preparation for the Methyl Linoleate compound was downloaded from the Molview.org tool for converting PDB databases, and the protein taken from the RCSB database was downloaded as PDB file for docking process. The MLL molecules exhibit binding energy of -4.49 kcal/mol, which shows maximum negative binding energy and indicates strong binding energy in ligant-protein interaction. The binding residues 4HOE show ALA 115 (O...HN), Estimated Inhibition Constant 514.52 μm and Reference RMSD value 28.52 Å were listed in Table 10. Those values represent a good docking score, and the title molecules show a good inhibitor of the 4HOE receptor with one hydrogen bond distance value of 2.0 Å against Candida albicans as shown in Fig. 10 that is related to stable ligand-protein interaction successively.

Table 7
UV- Vis Excitation Energy and Oscillator Strengths on MIP

States	B3LYP/6-311++G(d,p) Gas Phase			Experimental (nm)	Major Contributions Energy (%)
	Absorption band λ (nm)	Excitation energies (eV)	Oscillation Strength		
S1	225.75	5.492	1.1322	226	HOMO->LUMO (99%)
S2	212.51	5.834	0.0007	-	H-1->L+1 (98%)
S3	210.92	5.878	0.0000	-	HOMO->L+1 (99%)

Table 8
Thermodynamic parameters at different temperatures on MLL

T(K)	S(J/mol.K)	C(J/mol.K)	H(kJ/mol)
100	493.602	206.347	13.062
200	665.492	297.927	38.378
298.15	802.843	400.617	72.475
300	805.327	402.74	73.218
400	937.185	519.528	119.333
500	1065.034	628.057	176.829
600	1188.02	721.295	244.427
700	1305.294	800.078	320.605
800	1416.612	866.926	404.045
900	1522.106	924.042	493.667
1000	1622.067	973.093	588.585

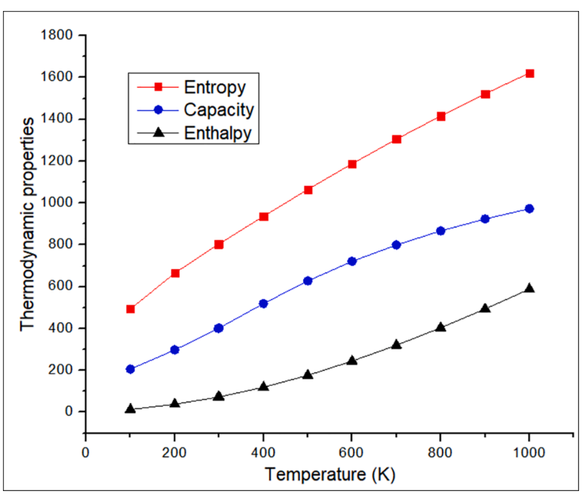

Fig. 9. Compared Graph of thermodynamic parameters at different temperature on MLL

5.2. Conclusion

The Methyl Linoleate was synthesized from the methanol crude of L. AegleMarmelos and identified from the GC-MS result. The optimized geometry structure of MLL was compared with XRD values and The Potential Energy Scan (PES) exhibit the conformational stability at minimum energy. The FT-IR spectra with intensity observed and the calculated wavenumber with PED% were carried out in the Veda 04 program. Both theoretical and experimental spectra are confirmed by good qualitative agreements. The UV-Vis spectra observed at 225 nm and well correlated with the DT-DFT computed by 226 nm. The MEP plot exhibits electrophilic attack in carbon dioxide group (donor) and nucleophilic attack in the methyl group (acceptor) and Muliken population analysis on the MLL compound was also calculated. The HOMO-LUMO transition revealed an energy gap of 5.3315 eV for high stability and low reactivity, which is related to more biological activity. The NBO investigate strong conjugate interaction exhibit $(\sigma)O_{20}\rightarrow(\pi^*)$ C1-C_{19} with more stabilization energy (49.20 Kcal/mol). The thermodynamic properties were estimated at various temperatures from 100 -1000 k. The chemical shift values of proton and carbon NMR in DMSO was calculated. The MLL molecules showed good inhibitor of the 4HOE receptor against Candida albicans, corresponding to stable ligand-protein interactions successively.

Table 9
Theoretical NMR Chemical Shift values of MLL

Atom	Theoretical chemical shift in ppm	Atom	Theoretical chemical shift in ppm
C_1	155.01	H_{43}	3.56
C_{10}	124.87	H_{36}	3.55
C_{13}	116.22	H_{37}	3.55
C_{11}	114.82	H_{22}	3.45
C_{12}	114.32	H_{23}	3.45
C_{21}	42.67	H_{25}	3.11
C_{16}	32.77	H_{24}	3.11
C_6	31.78	H_{44}	2.78
C_7	31.53	H_{45}	2.77
C_5	31.38	H_{48}	2.74
C_8	30.38	H_{49}	2.74
C_{15}	30.33	H_{28}	2.71
C_4	30.13	H_{29}	2.69
C_2	29.25	H_{34}	2.68
C_9	28.81	H_{35}	2.68
C_{14}	28.09	H_{50}	2.64
C_3	26.80	H_{30}	2.62
C_{17}	23.62	H_{31}	2.62
C_{18}	13.13	H_{46}	2.59
H_{39}	7.95	H_{47}	2.59
H_{40}	6.92	H_{32}	2.57
H_{38}	6.48	H_{33}	2.57
H_{41}	6.15	H_{26}	2.47
H_{55}	5.06	H_{27}	2.47
H_{54}	5.06	H_{51}	2.33
H_{53}	4.80	H_{52}	2.33
H_{42}	3.56		

Credit author statement

C.Prabhu[1]
Conceptualization, Methodology
P.Rajesh[2]*,
Methodology, Writing - Original Draft, Writing - Review & Editing
E.Dhanalakshmi[3]*,
Conceptualization, Writing – Review, Software (Docking studies)
T. Gnanasambandan[4]
Software, Validation
M.Priyadharshini[5]
Data curation

Table 10
Shows the Binding affinity of the proteins using AUTODOCK software.

Protein (PDB ID)	Bonded residues	No. of hydrogen bond	Bond distance (Å)	Estimated Inhibition Constant (μm)	Binding energy (kcal/mol)	Reference RMSD (Å)
4HOE	ALA 115 (O...HN)	1	2.0	514.52	-4.49	28.52

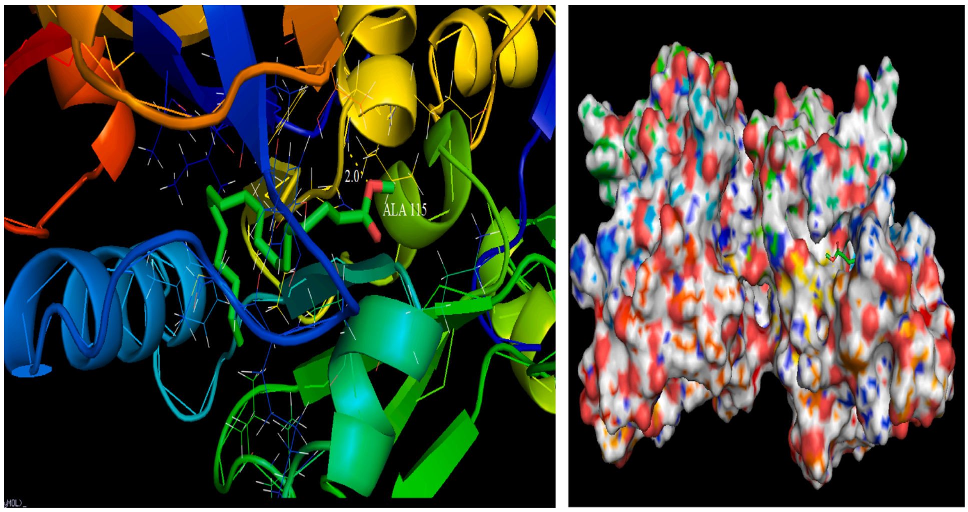

Fig. 10. Ribbon shape indicates protein (4HOE) and ligand-Docking complex are seen in the active site ALA 115 amino acid.

Declaration of Competing Interest

The authors declare that they have no known competing financial interests or personal relationships that could have appeared to influence the work reported in this paper.

Data availability

Data will be made available on request.

References

[1] Ramveer Singh, Ajeet Singh, Neelesh Babu and Navneet, Ethno-medicinal and Pharmacological activities of *Aegle marmelos* (Linn.) Corr: a review, J. Pharm. Innov. 8 (6) (2019) 176–181.

[2] Chamila Kumari Pathirana, Terrence Madhujith, Janakie Eeswara, Bael (*Aegle marmelos* L. Corrêa), a medicinal tree with immense economic potentials, Adv. Agric. (2020) 1–13, https://doi.org/10.1155/2020/8814018.

[3] Babita Veer, Ram Singh, Phytochemical screening and antioxidant activities of *Aegle marmelos* leaves, TACL 9 (2019) 478–485, https://doi.org/10.1080/22297928.2019.1657946.

[4] Shikha Raheja, Amit Girdhar, Anjoo Kamboj, Viney Lather, Deepti Pandita, *Aegle marmelos* leaf extract ameliorates the cognitive impairment and oxidative stress induced by intracerebroventricular streptozotocin in male rats, Life Sci. (2019) 1–20, https://doi.org/10.1016/j.lfs.2019.02.032.

[5] K. Jagajjanani Rao, Santanu Paria, Green synthesis of silver nanoparticles from aqueous *Aegle marmelos* leaf extract, Mater. Res. Bull. (2012) 1–28, https://doi.org/10.1016/j.materresbull.2012.11.035.

[6] Mohana Sriramulu, Dhananjay Shukla, Shanmugam Sumathi, *Aegle marmelos* leaves extract mediated synthesis of zinc ferrite: antibacterial activity and drug delivery, Mater. Res. Express. 5 (2018), 115404.

[7] Bing Tan, Natthakarn Chiranthanut, Sunee Chansakaow, Seewaboon Sireeratawong, Parirat Khonsung, Wutigri Nimlamool, Mingkwan Na Takuathung, Nirush Lertprasertsuke, Anti-inflammatory effects of Pikad Tri-phol-sa-mut-than remedy, consisting of dried fruits of *Aegle marmelos* (L.) Corrêa, *Coriandrum sativum* L., and *Morinda citrifolia* L, J. Ethnopharmacol. 298 (2022), https://doi.org/10.1016/j.jep.2022.115639.

[8] Wasim Ahmad, Mohd Amir, Adil Ahmad, Abuzer Ali, Amena Ali, Shadma Wahab, Harshita Abul Barkat, Mohammad Azam Ansari, Mohammad Sarafroz, Ayaz Ahmad, Md.Abul Barkat, Prawez Alam, *Aegle marmelos* leaf extract phytochemical analysis, cytotoxicity, *in vitro* antioxidant and antidiabetic activities, Plants 10 (2021), https://doi.org/10.3390/plants10122573.

[9] Gattu Sampath, Muthusamy Govarthanan, Neelamegam Rameshkumar, N. DaiViet, Muthukalingan Krishnan, Palaniappan Sivasankar, Nagarajan Kayalvizhi, Ecofriendly biosynthesis metallic silver nanoparticles using *Aegle marmelos* (Indian bael) and its clinical and environmental applications, Appl. Nanosci. 13 (2023) 663–674, https://doi.org/10.1007/s13204-021-01883-8.

[10] Ravi Babu Birudu, Padmavathi Pamulapati, Sathish Kumar Manoharan, Evaluation of biochemical changes in diabetic rats treated with *Aegle marmelos* (L.) methanolic leaf extract, Pharmacogn. Res. 12 (2020), https://doi.org/10.4103/pr.pr_53_19.

[11] Ritu Tiwari, Tusha Tripathi, Yasir A. Khan, Annie Gupta, Mahaveer Dhobi, Sushma Srivastava, Brahmanand Singh, Karuna Shanker, Vivekanadan Kalaiselvan, Gyanendra N Singh, Metabolite profiling, isolation of cyclic polyols, antioxidant and anti-inflammatory activities of *Aegle marmelos*: NMR and GC–MS based metabolomics study, J Herbs Spices Med Plants 27 (2020) 68–82, https://doi.org/10.1080/10496475.2020.1786873.

[12] M.Govindaraju P.Vennila, G. Venkatesh, C. Kamal, Y. Sheena Mary, C. Yohannan Panicker, S. Kaya, Stevan Armakovic, Sanja J. Armakovic, A complete computational and spectroscopic study of 2-bromo-1, 4-dichlorobenzene - a frequently used benzene derivative, J. Mol. Struct. 1151 (2018) 245–255, https://doi.org/10.1016/j.molstruc.2017.09.049.

[13] A. Suvitha, S. Periandy, S. Boomadevi, M. Govindarajan, Vibrational frequency analysis, FT-IR, FT-Raman, ab initio, HF and DFT studies, NBO, HOMO–LUMO and electronic structure calculations on pycolinaldehyde oxime, Spectrochim, Acta A Mol. Biomol. Spectrosc. 117 (2014) 216–224, https://doi.org/10.1016/j.saa.2013.07.080.

[14] Stevan Armakovic, Sanja J. Armakovic, Jovan P. Setrajcic, Vladimir Holodkov, Aromaticity, response, and nonlinear optical properties of sumanene modified with boron and nitrogen atoms, J. Mol. Model. (2014) 1–13, https://doi.org/10.1007/s00894-014-2538-4.

[15] S. Premkumar, A. Jawahar, T. Mathavan, M. Kumara Dhas, A. Milton Franklin Benial, Vibrational spectroscopic and DFT calculation studies of 2-amino-7-bromo-5- oxo-[1]benzopyrano [2,3-b]pyridine-3 carbonitrile, Spectrochim. Acta A Mol. Biomol. Spectrosc. (2014), https://doi.org/10.1016/j.saa.2014.11.029.

[16] V.V. Aswathy, Sheena Mary Y, C.Yohannan Panicker P.J.Jojo, Anna Bielenica, Stevan Armakovic, Sanja J. Armakovic, Paulina Brzozka, Sylwester Krukowski, C. Van Alsenoy, Investigation of spectroscopic, reactive, transport and docking properties of 1-(3,4- dichlorophenyl)-3-[3-(trifluoromethyl)phenyl]thiourea (ANF-6): combined experimental and computational study, J. Mol. Struct. 1134 (2017) 668–680, https://doi.org/10.1016/j.molstruc.2017.01.016.

[17] Jinxiang You, Jing Wang, Shuhui Zhang, Jun Luo, Zhiwei Peng, Mingjun Rao, Guanghui Li, Thermodynamic properties of Na_2MgSiO_4: DFT calculation and experimental validation, Calphad 79 (2022), https://doi.org/10.1016/j.calphad.2022.102480.

[18] Ernest C. Agwamba, Akaninyene D. Udoikono, Hitler Louis, Esther U. Udoh, Innocent Benjamin, Azuaga T. Igbalagh, Henry O. Edet, Emmanuel U. Ejiofor, B. Ugi, Ushaka, synthesis, characterization, DFT studies, and molecular modeling of azo dye derivatives as potential candidate for trypanosomiasis treatment, Chem. Phys. Impact. 4 (2022), https://doi.org/10.1016/j.chphi.2022.100076.

[19] Celal Tugrul Zeyrek, Selen Bilge Kocak, Huseyin Unver, Serhan Pektas, Nisan Sevin Bas¸ terzi, Omer Celik, Molecular structure and density functional modelling studies of 2-[(E)-2-(4-hydroxyphenyl)ethyliminomethyl]phenol, J. Mol. Struct. 1100 (2015) 570–581, https://doi.org/10.1016/j.molstruc.2015.07.068.

[20] Stevan Armakovi, Sanja J. Armakovi, Jovan P. Setraj, Hydrogen storage properties of sumanene, Int. J. Hydrog. 38 (2013) 12190–12198, https://doi.org/10.1016/j.ijhydene.2013.05.091.

[21] N. Kanagathara, R. Nanmaran, Illustration of potential energy surface from DFT calculation along with fuzzy logic modelling for optimization of N-acetylglycine, Comput. Theor. Chem. 1202 (2021), https://doi.org/10.1016/j.comptc.2021.113301.

[22] S. Kanchana, T. Kaviya, P. Rajkumar, M.Dhinesh Kumar, N. Elangovan, S. Sowrirajan, Computational investigation of solvent interaction (TD-DFT, MEP, HOMO-LUMO), wavefunction studies and molecular docking studies of 3-(1-(3-(5-((1-methylpiperidin-4-yl)methoxy)pyrimidin-2-yl) benzyl)-6-oxo-1,6-dihydropyridazin-3-yl)benzonitrile, Chem. Phys. Impact. 7 (2023), https://doi.org/10.1016/j.chphi.2023.100263.

[23] Ahmed Aj. Jabbar, Fuad O. Abdullah, Kamaran K. Abdulrahman, Yaseen Galali, Abdullah Sh, Sardar, GC–MS analysis of bioactivecompounds in methanolic extracts of papaver decaisnei and determination of its antioxidants and anticancer activities, J. Food Qual. (2022) 1–12, https://doi.org/10.1155/2022/1405157.

[24] Saraswathi Krishna, Sivaraj Chandrasekaran, Dhivya Dhanasekar, Arumugam Perumal, GCMS analysis, antioxidant and antibacterial activities of ethanol extract of *Anisomeles malabarica* (L.) R.Br. ex. Sims leaves, Asian J. Pharm 5 (2019) 180–187, https://doi.org/10.31024/ajpp.2019.5.1.26.

[25] B. Sathya, M. Prasath, M. Selvapandiyan, K. Prabha, Vibrational analysis (FT-IR and FT-Raman Spectra) and molecular docking evaluation of MPTB in GABA receptor, J. Clust. Sci. (2019), https://doi.org/10.1007/s10876-019-01562-3.

[26] P. Rajesh, S. Gunasekaran, T. Gnanasambandan, S. Seshadri, Molecular structure and vibrational analysis of Trifluoperazine by FT-IR, FTRaman & UV–vis spectroscopies combined with DFT calculations, Spectrochim. Acta A Mol. Biomol. Spectrosc. (2014), https://doi.org/10.1016/j.saa.2014.08.100.

[27] Anatoly Mishnev, Egils Bisenieks, Ilona Mandrika, Ramona Petrovska, Zenta Kalme, Imanta Bruverea, Gunars Dubursa, Crystal structure and metabolic activity of 4-(thien2-yl)-2-methyl-5-oxo-1,4,5,6,7,8-hexahydroquinoline-3-carboxylic acid ethoxycarbonylphenylmethyleste, Acta Cryst 74 (2018) 1577–1579, https://doi.org/10.1107/S2056989018014251.

[28] S. Janani, Hemamalini Rajagopal, S. Muthu, S. Aayisha, M. Raja, Molecular structure, spectroscopic (FT-IR, FT-Raman, NMR), HOMO-LUMO, chemical reactivity, AIM, ELF, LOL and molecular docking studies on 1-Benzyl-4-(N-Boc-amino)piperidine, J. Mol. Struct. 1230 (2021), https://doi.org/10.1016/j.molstruc.2020.129657.

[29] Vahidreza Darugar, Mohammad Vakili, Sayyed Faramarz Tayyari, Poul Erik Hansen, Fadhil S. Kamouna, Molecular structure, intramolecular hydrogen bond strength, vibrational assignment, and spectroscopic insight of 4-phenylamino-3-penten-2- one and its derivatives: a theoretical and experimental study, Mol. Liq. 334 (2021), 116035, https://doi.org/10.1016/j.molliq.2021.116035.

[30] M. Govindamma, M. Prasath, S. Kamaraj, B. Sathya, *In vivo*, molecular docking, spectroscopy studies of (S)-2,3-dihydro-5,7- dihydroxy-2(3-hydroxy-4-methoxyphenyl)-4H-1-benzopyran-4-one: a potential uptake PI3/AKT inhibitor, Biocatal. Agric. Biotechnol. 18 (2019), https://doi.org/10.1016/j.bcab.2019.101086.

[31] S. Suresh, S. Gunasekaran, S. Srinivasan, Spectroscopic (FT-IR, FT-Raman, NMR and UV–visible) and quantum chemical studies of molecular geometry, Frontier molecular orbital, NLO, NBO and thermodynamic properties of salicylic acid, Spectrochim. Acta A Mol. Biomol. Spectrosc. 132 (2014) 130–141, https://doi.org/10.1016/j.saa.2014.04.174.

[32] S. Suresh, S. Gunasekaran, S. Srinivasan, Vibrational spectra (FT-IR, FT-Raman), frontier molecular orbital, first hyperpolarizability, NBO analysis and thermodynamics properties of Piroxicam by HF and DFT methods, Spectrochim. Acta A Mol. Biomol. Spectrosc. 138 (2015) 447–459, https://doi.org/10.1016/j.saa.2014.11.040.

[33] P. Rajesh, S. Gunasekaran, T. Gnanasambandan, S. Seshadri, Experimental, quantum chemical and NBO/NLMO investigations of pantoprazole, Spectrochim. Acta A Mol. Biomol. Spectrosc. 136 (2015) 247–255, https://doi.org/10.1016/j.saa.2014.09.029.

[34] K. Arulvani, R. Venkateswaramoorthi, S. Gunavathi, S. Bharanidharan, Synthesis, crystal structure, Hirshfeld surface, biological evaluation, DFT and molecular docking studies of unsymmetrical 3-allyl-5-ethyl-1,4- dihydro-2,6-dimethyl-4-phenyl pyridine-3,5- dicarboxylate derivatives, Mol. Phys. (2023), https://doi.org/10.1080/00268976.2023.2200845.

[35] Atse Adepo Jacques, Kone Soleymane, Diomande Sékou, Et Bamba El-Hadji Sawaliho, NBO Analysis by ONIOM and DFT (B3LYP) Calculations of Intramolecular and Intermolecular Interactions of Artemisinin, Quinine and Thirteen Manzamenones with H2O or Alanine, J. Mater. Sci. Chem. Eng. 10 (2022) 78–98, https://doi.org/10.4236/msce.2022.1010006.

[36] Abhijit R. Bukane, Bapu S. Jagdale, DFT exploration on molecular characteristics of 6-methyl-2-oxo-4-phenyl-1,2,3,4- tetrahydropyrimidine-5-carboxylate, J. Adv. Chem. Sci. 7 (2021) 717–720, https://doi.org/10.30799/jacs.236.21070105.

[37] S. Rohit, Shinde, Ultrasound assisted synthesis, molecular structure, UV visible assignments, MEP and Mulliken charges study of (E)-3-(4-chlorophenyl)-1-(4-methoxyphenyl)prop-2-en-1-one: experimental and DFT correlational, Mat. Sci. Res. 18 (2021) 86–96, https://doi.org/10.13005/msri/180110. Doi:.

[38] P.Myvizhi S.Bharanidharan, Frontier molecular orbitals (FMO) and molecular electrostatic potential (MEP) surface of 2-(4-chlorophenyl)-1-((furan-2-yl) methyl)-4,5-dimethyl1H-imidazole using DFT method, Int J Pure Appl 119 (2018) 6769–6777.

[39] C. Dabora Vincy, J.D. Deephlin Tarika, X.D. Divya Dexlinc, A. Rathika, T. Joselin Beaula, Exploring the antibacterial activity of 1, 2 diaminoethane hexanedionic acid by spectroscopic, electronic, ELF, LOL, RDG analysis and molecular docking studies using DFT method, J. Mol. Struct. 1247 (2022), 131388, https://doi.org/10.1016/j.molstruc.2021.131388.

[40] Vishnu A. Adole, DFT calculations on three 2,3-dihydrobenzofuran linked chalcones: structural, HOMO-LUMO and spectroscopic (UV–vis and IR) interpretation, Vietnam J. Chem. 61 (2022), https://doi.org/10.1002/vjch.202100023.

[41] Yousif Hussein Azeez, Seda Hekim, Sinan Akpinar, The theoretical investigation of the HOMO, LUMO energies and chemical reactivity of C9H12 and C7F3NH5Cl molecules, JPCFM 2 (2019) 29–31.

[42] S.K. Pathak, R. Srivastava, A.K. Sachan, O. Prasad, L. Sinha, A.M. Asiri, M. Karabacak, Experimental (FT-IR, FT-Raman, UV and NMR) and quantum chemical studies on molecular structure, spectroscopic analysis, NLO, NBO and reactivity descriptors of 3,5-Difluoroaniline, Spectrochim. Acta A Mol. Biomol. Spectrosc. 135 (2015) 283–295, https://doi.org/10.1016/j.saa.2014.06.149.

[43] M. Habib Rahuman, S. Muthu, B.R. Raajaraman, M. Raja, H. Umamahesvari e, Investigations on 2-(4-Cyanophenylamino) acetic acid by FT-IR,FT-Raman, NMR and UV–vis spectroscopy, DFT (NBO, HOMO-LUMO, MEP and Fukui function) and molecular docking studies, Heliyon 6 (2020), https://doi.org/10.1016/j.heliyon.2020.e04976.

[44] S. Aayisha, T.S. Renuga Devi, S. Janani, S. Muthu, M. Raja, S. Sevvanthi, DFT, molecular docking and experimental FT-IR, FT-Raman, NMR inquisitions on "4-chloro-N-(4,5-dihydro-1H-imidazol-2-yl)-6- methoxy-2-methylpyrimidin-5-amine": alpha-2-imidazoline receptor agonist antihypertensive agent, J. Mol. Struct. 1186 (2019) 468–481, https://doi.org/10.1016/j.molstruc.2019.03.056.

[45] Queen S. Obua, Hitler Louis, Joseph O. Odeya, Ishegbe Joyce Eko, Shuaibu Abdullahi, Tabe N. Ntui, Ofiong E. Offiong, Synthesis, spectra (FT-IR, NMR) investigations, DFT study, in silico ADMET and Molecular docking analysis of 2-amino-4-(4-aminophenyl)thiophene-3-carbonitrile as a potential anti-tubercular agent, J. Mol. Struct. 1244 (2021), https://doi.org/10.1016/j.molstruc.2021.130880.

[46] Mohammad Jane Alam, Azhar U. Khan, Mahboob Alam, Shabbir Ahmad, Spectroscopic (FTIR, FT-Raman, 1 H NMR and UVeVis) and DFT/TD-DFT studies on cholesteno [4,6-b,c]-20,50 -dihydro-10,50 –benzothiazepine, J Mol Struct 1178 (2019) 570–582, https://doi.org/10.1016/j.molstruc.2018.10.063.

[47] Haroldo C. da Silva, Wagner B. de Almeida, Theoretical calculations of 1 H NMR chemical shifts for nitrogenated compounds in chloroform solution, Chem. Phys. 528 (2020), https://doi.org/10.1016/j.chemphys.2019.110479.

[48] Phineus R.L. Markwick, Michael Nilges, Computational approaches to the interpretation of NMR data for studying protein dynamics, Chem. Phys. 396 (2012) 124–134, https://doi.org/10.1016/j.chemphys.2011.11.023.

[49] Saira Naseem, Muhammad Khalid, Muhammad Nawaz Tahir, Mohammad A. Halim, Ataualpa A.C. Braga, Muhammad Moazzam Naseer, Zahid Shafiq, Synthesis, structural, DFT studies, docking and antibacterial activity of a xanthene based hydrazone ligand, J. Mol. Struct. (2017), https://doi.org/10.1016/j.molstruc.2017.04.093.

[50] Mustapha Ait El Had, Mouhi Eddine Hachim, Said Byadi, Lahoucine Bahsis, Abdelouahd Oukhrib, Hafid Anane, Lahcen El Ammari, Mohamed Saadi, Moha Berraho, Ahmed Benharref, Moha Taourirte, A newly synthesized β-amino-α, β-unsaturated ketone derivative of β-himachalene: structural, NBO, NLO, and molecular docking studies, Biointerface Res. Appl. Chem. 13 (2023) 83, https://doi.org/10.33263/BRIAC131.083.